ResearchGate

See discussions, stats, and author profiles for this publication at: https://www.researchgate.net/publication/231206568

Calibration-Free Optical Chemical Sensors

ARTICLE *in* ANALYTICAL CHEMISTRY · FEBRUARY 1999

Impact Factor: 5.64 · DOI: 10.1021/ac9805955

CITATIONS
76

READS
50

2 AUTHORS, INCLUDING:

Mike DeGrandpre
University of Montana
84 PUBLICATIONS **1,917** CITATIONS

SEE PROFILE

Available from: Mike DeGrandpre
Retrieved on: 16 January 2016

Anal. Chem. **1999,** *71,* 1152−1159

Calibration-Free Optical Chemical Sensors

Michael D. DeGrandpre*,† and Matthew M. Baehr‡

Department of Chemistry, The University of Montana, Missoula, Montana 59812

Terence R. Hammar§

Department of Applied Ocean Physics and Engineering, Woods Hole Oceanographic Institution, Woods Hole, Massachusetts 02543

Calibrations are necessary for most chemical sensors because the response is not consistent between sensors nor stable over time. If chemical sensors could be designed to have identical behavior from sensor to sensor and no drift, the need for sensor calibrations would be reduced. In the present paper, the feasibility of calibration-free optical chemical sensors is explored. An indicator-based pCO_2 (partial pressure of CO_2) sensor is designed that has excellent sensor-to-sensor reproducibility and measurement stability. This superior level of performance is achieved by using the following strategy: (1) renewing the sensing solution, (2) allowing the sensing solution to reach equilibrium with the analyte, (3) calculating the response from a ratio of the indicator solution absorbances, and (4) through careful solution preparation, wavelength calibration, and stray light rejection. Three pCO_2 sensors are calibrated, and the response curves are essentially identical within the uncertainty of the calibration. Long-term laboratory and field studies are presented that show the response has no drift over extended periods (months). The theoretical response, determined from thermodynamic characterization of the indicator solution, also predicts the observed calibration-free performance. Other absorbance-based sensors, such as optrodes, can be designed and operated in a similar fashion, making calibration-free optical chemical sensors available for a wide range of biomedical, industrial, and environmental applications.

Research on optical chemical sensors blossomed over the past 15−20 years as a result of the availability of novel and inexpensive waveguides and the ever-increasing need for sensors for a wide range of chemical applications. Two general groups of optical chemical sensors evolved from this work, those that directly probe a spectrochemical property of the sample and those that utilize an analyte-selective reagent to transduce analyte concentration into an optical signal. The present study focuses on the latter group, reagent-based optical chemical sensors (ROCS). ROCS generated substantial excitement early in their development because they promised improved performance and versatility over their electrochemical sensor analogs. These potential advantages included greater stability and selectivity and a simple, characterizable response. But, after nearly 20 years of research and development, these advantages have yet to be fully realized.[1,2] Our work in this area has focused on the development of ROCS for autonomous mooring-based measurements of seawater pCO_2,[3−5] a demanding application that, to be successful, had to avoid the shortcomings of earlier ROCS designs. The pCO_2 sensor developed from these efforts, based on a renewable-reagent design described below, demonstrated excellent long-term stability.[5] These results, in combination with theoretical predictions, suggested that the sensors could circumvent the need for periodic calibrations. We show here through sensor intercomparisons and long-term studies of the sensor response that calibration-free operation is indeed feasible. The conclusions drawn from this study have potential implications for all absorbance and fluorescence-based chemical sensors that operate in equilibrium with the analyte.

BACKGROUND

The majority of ROCS use fiber optics to direct light into a small membrane-enclosed volume, resulting in single-ended electrode-like probes.[6] In most ROCS designs, a colorimetric or fluorometric reagent is entrapped within the membrane at the fiber tips. The membrane serves a variety of important purposes—it contains and protects the analyte-selective reagent, it provides an additional level of selectivity for groups of different compounds (e.g., gases, hydrophilic or hydrophobic species), and it acts as a diffuse reflector of the light transmitted through, or emitted from, the selective reagent. Chemical sensing is generally accomplished by simply monitoring the change in light intensity in the presence of the analyte of interest. Light intensity changes unrelated to the analyte such as light source fluctuations or changes in the fiber optic transmission are compensated for by using a reference light intensity at a wavelength insensitive to the analyte concentration.

† (E-mail) mdegrand@selway.umt.edu; (fax) 406-243-4227.
‡ (E-mail) mbaehr@selway.umt.edu.
§ (E-mail) thammar@whoi.edu.

(1) MacCraith, B. D.; McDonagh, C.; McEvoy, A. K.; Butler, T.; O'Keefe, G.; Murphy, V. *J. Sol-Gel Sci. Technol.* **1998**, *8*, 1053−1061.
(2) Spichiger-Keller, U. E. *Chemical Sensors and Biosensors for Medical and Biological Applications*; Wiley-VCH: Weinheim, 1998.
(3) DeGrandpre, M. D. *Proc. SPIE-Int. Soc. Opt. Eng.* **1991**, *1587*, 60−66.
(4) DeGrandpre, M. D. *Anal. Chem.* **1993**, *65*, 331−337.
(5) DeGrandpre, M. D.; Hammar, T. R.; Smith, S. P.; Sayles, F. L. *Limnol. Oceanogr.* **1995**, *40*, 969−975.
(6) Angel, S. M. *Spectroscopy* **1987**, *2*, 38−50.

10.1021/ac9805955 CCC: $18.00 © 1999 American Chemical Society
Published on Web 02/06/1999

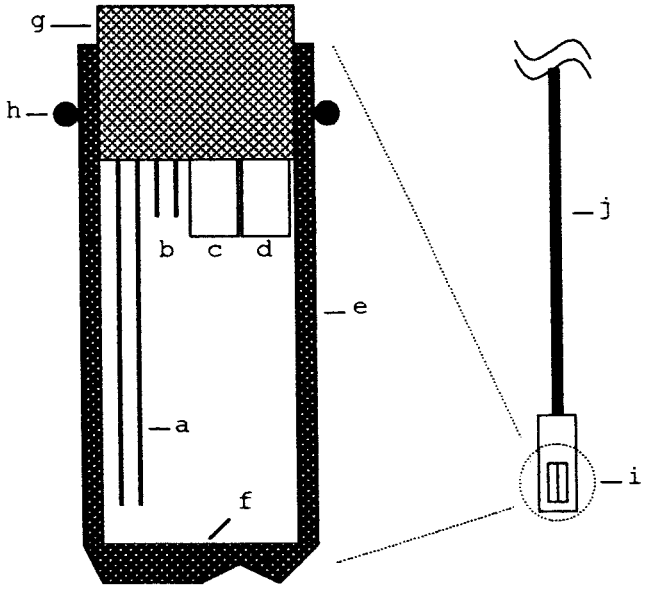

Figure 1. The original single-ended renewable-reagent pCO_2 sensor design described in refs 3 and 4. The sensor outer diameter is ~1 mm: (a) reagent delivery capillary tube; (b) reagent exit capillary tube; (c) fiber optic from source; (d) fiber optic to detection system; (e) white silicone rubber membrane; (f) white silicone sealant; (g) epoxy sealant; (h) O-ring; (i) sensor stainless steel housing; (j) fiber optic and capillary tubing cable. Note: individual components are not drawn to scale.

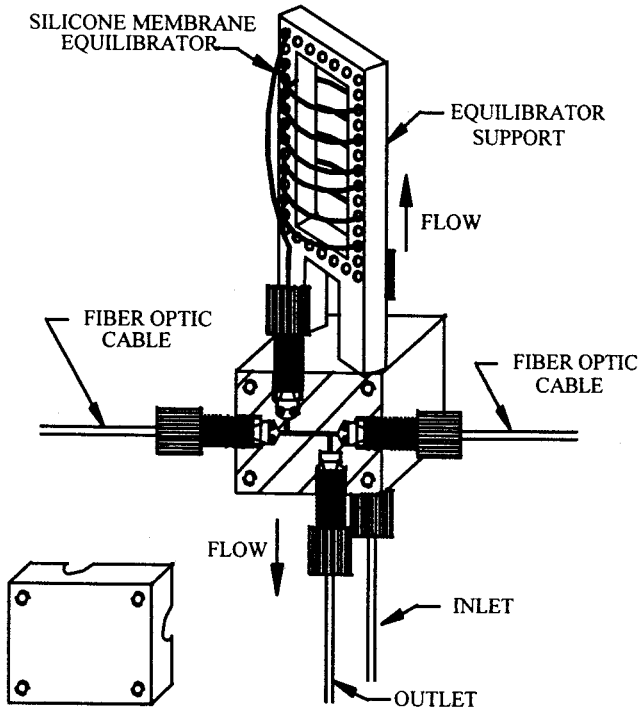

Figure 2. Cutaway view of the current SAMI-CO_2 sensor design based on a membrane-equilibrator and fiber optic flow cell.

Even so, these ROCS designs have significant stability problems that primarily originate from changes in the composition of the entrapped reagent chemistry.[1] To improve ROCS performance, researchers began investigating methods for renewing the reagent.[7,8] The promising results from these sensors led our group to explore the possibility of using a renewable-reagent approach for the measurement of seawater pCO_2.

The sensor, named the submersible autonomous moored instrument for CO_2 (SAMI-CO_2) was developed in the early 1990s.[3–5] The SAMI-CO_2 design is based upon previous CO_2 sensor designs that used a colorimetric pH indicator entrapped within a gas-permeable membrane.[9] However, unlike previous sensors, the reagent is renewed during each measurement cycle. The original single-ended probe design reported in refs 3 and 4 is shown in Figure 1. The ultimate limitation of the single-ended design in Figure 1 was its poor light throughput. A 10-W (5 V, 2 A) light source was required to obtain sufficient signal to noise (S/N), an inordinate power requirement for autonomous battery-powered applications. The sensor was subsequently redesigned, finally evolving into a transmission geometry (Figure 2). This face-to-face fiber configuration made it possible to use a 0.6-W (5 V, 0.115 A) lamp, greater than a 10-fold improvement in throughput for a S/N equivalent to that obtained with the previous design. Currently an 18 D-cell alkaline battery pack provides power for over 6 months of operation with 48 measurements per day (0.5-h resolution).[5]

(7) Berman, R. J.; Christian, G. D.; Burgess, L. W. *Anal. Chem.* **1990**, *62*, 2066–2071.
(8) Inman, S. M.; Stromvall, E. J.; Lieberman, S. H. *Anal. Chim. Acta* **1989**, *217*, 249–262.
(9) Vurek, G. G.; Fuestel, P. J.; Severinghaus, J. W. *Ann. Biomed. Eng.* **1983**, *11*, 499–510.

In taking steps to reduce the power requirements, the sensor began to look more and more like a conventional spectrophotometric cell. The resemblance was, perhaps, not a coincidence. We had hypothesized that if ROCS measurements are similar to a spectrophotometric measurement where true optical absorbances are obtained,

$$A_\lambda = -\log(I_\lambda / I_{\lambda 0}) \qquad (1)$$

where A_λ is the indicator solution absorbance at wavelength λ, I_λ is the intensity transmitted through the reagent solution, and $I_{\lambda 0}$ is the intensity transmitted through a blank solution, the sensor could achieve stability and accuracy comparable to conventional spectrophotometric measurements. Based on theoretical calculations (described below), additional performance improvements could be obtained by using a ratio of indicator optical absorbances at two different wavelengths. The calculated absorbance ratios should be dependent on only a few operational parameters, and if these parameters are reproducible and stable, ROCS could operate with an identical and drift-free response, making calibrations unnecessary. These ideas were implemented in the design of SAMI-CO_2 as described in the following section.

OPERATING PRINCIPLE

The SAMI-CO_2 sensor is essentially a membrane equilibrator attached to a fiber optic flow cell (Figure 2) (the sensor dimensions and other specifications have been reported previously).[5] The ambient CO_2 diffuses through a tubular silicone rubber membrane into a sulfonephthalein indicator solution. The diffusion of CO_2 into the indicator solution leads to the formation of carbonic acid, which changes the solution pH thereby establishing the

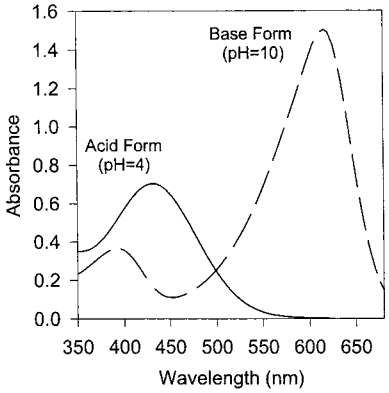

Figure 3. Absorbance spectra of the acid (HL^-) and base (L^{2-}) forms of the sulfonephthalien indicator bromothymol blue used in the SAMI-CO_2. The total indicator concentration was $\sim 9.0 \times 10^{-5}$ M.

equilibrium concentrations of the acid (HL^-) and base (L^{2-}) forms of the indicator:

$$HL^- \overset{K_a}{\rightleftharpoons} L^{2-} + H^+ \tag{2}$$

The fully protonated form of the diprotic sulfonephthalein indicator (H_2L, $pK_a = 2$) is not present in significant amounts at the indicator solution pH (pH ~7). Indicator solution stored in an isolated reagent bag is pumped into the membrane for each measurement. In initial studies using the design in Figure 1, the indicator solution was pumped at a rate that did not allow full equilibration with the external CO_2, resulting in a diffusion-dependent response. Although this approach had excellent CO_2 sensitivity, slow or stopped-flow, which achieved equilibrium with the external solution, was less sensitive to flow rate and temperature and resulted in dramatically improved measurement precision.[4] The sensor design in Figure 2 requires ~5 min to achieve equilibrium between the indicator and external solution.[5] During each measurement cycle, a solenoid pump is activated pushing new indicator solution into the membrane and flushing the CO_2-equilibrated solution into the fiber optic flow cell.[5] The SAMI solenoid pump delivers ~50 μL of solution per pulse, which is sufficient to flush out the cell and membrane.

As indicated above, the sensor response is calculated from the indicator absorbances at two different wavelengths. The wavelengths chosen correspond to the molar absorptivity maximums of the two indicator forms. For bromothymol blue (BTB), the sulfonephthalien indicator used in the SAMIs, the wavelengths are 434 nm for the acid, or protonated HL^- form, and 620 nm for the base, or unprotonated L^{2-} form (Figure 3). The sensor response could be based on the individual absorbances at either 434 or 620 nm, but by combining the absorbances in a ratio, i.e., A_{620}/A_{434}, the response should be independent of cell path length and total indicator concentration, two potential sources of variability and drift. Furthermore, temperature dependence is dampened due to the similarity of the temperature coefficient of the individual molar absorptivities.[10]

The SAMI response is calculated using an equation that relates the absorbance ratio, A_{620}/A_{434}, directly to the indicator solution pH. The solution pH at infinite dilution (activity coefficients, 1) can be described using a combination of the indicator equilibrium expression with Beer's law,[10,11]

$$pH = pK_a + \log([L^{2-}]/[HL^-]) \tag{3}$$

with

$$\frac{[L^{2-}]}{[HL^-]} = \frac{A_R - \epsilon_{620a}/\epsilon_{434a}}{\epsilon_{620b}/\epsilon_{434a} - A_R\epsilon_{434b}/\epsilon_{434a}} \tag{4}$$

where $A_R = A_{620}/A_{434}$ and the subscripted ϵ's represent the molar absorptivities for BTB with "a" the acid form of the indicator and "b" the base form of the indicator. As shown in Figure 3, the absorbance spectra for the acid and base forms overlap and both indicator forms contribute to the absorbances at the analytical wavelengths. These overlapping absorbances are accounted for in the derivation of eq 4.

The SAMI response, R_{CO_2}, is calcuated from eqs 3 and 4:

$$R_{CO_2} = -\log\left(\frac{A_R - \epsilon_{620a}/\epsilon_{434a}}{\epsilon_{620b}/\epsilon_{434a} - A_R\epsilon_{434b}/\epsilon_{434a}}\right) = pK_a - pH \tag{5}$$

The response therefore has a physical meaning, representing the indicator solution pH offset from the pK_a. Equation 5 also shows that the response R_{CO_2} is only dependent upon the molar absorptivities and absorbance ratio. In turn, the absorbance ratio A_R is dependent upon the original solution alkalinity, ambient pCO_2, and temperature. From eq 5 it can be hypothesized that every SAMI should have an identical pCO_2 response for an identical indicator solution, assuming good wavelength and absorbance accuracy.

However, to calculate A_R the optical absorbances (eq 1) at 434 and 620 nm must be determined, which requires measurement of the intensity that passes through a blank solution ($I_{\lambda 0}$). Flushing the blank through the sensor plumbing consumes significant time, power, and indicator solution. To minimize these practical limitations, solution blanks are determined intermittently and a "blank constant" (K_λ) is employed so that the absorbances can be calculated between blank measurements. The indicator absorbance is calculated using,

$$A_\lambda = -\log(I_\lambda/I_{ref}K_\lambda) \tag{6}$$

where I_{ref} is the transmitted light intensity at a wavelength where the indicator does not appreciably absorb (740 nm) and $K_\lambda = I_{\lambda 0}/I_{ref}$ is determined from the most recent blank measurement. By using I_{ref} at 740 nm for every measurement, the sensor corrects for light intensity fluctuations from the source and changes in the transmittance of fibers and optical cell. During field deployments, blanks are typically run every 2−3 days or after ~100−150 measurements.

SAMI THEORETICAL RESPONSE

Past modeling efforts proved helpful in optimizing the composition of the SAMI indicator solution.[4] In the present research,

(10) Byrne, R. H.; Breland, J. A. *Deep-Sea Res.* **1989**, *36*, 803−810.

(11) Clayton, T. D.; Byrne, R. H. *Deep-Sea Res.* **1993**, *40*, 2115−2129.

an equilibrium model is used to evaluate whether the experimental response is following expected behavior. This comparison helps determine whether there are any systematic instrument-related errors in the SAMI response. The theoretical calculations are also useful for predicting the sensor temperature sensitivity, which is important for understanding and correcting the sensor temperature dependence.

The theoretical response is equal to the difference between the indicator pK_a and solution pH as shown on the right side of eq 5. The theoretical response is a fundamental thermodynamic property of the indicator solution and is independent of instrument settings. The pH in eq 5 is dependent upon pCO_2, and this relationship was derived from the indicator and carbonic acid equilibria and solution charge balance,

$$[H^+]^3 + [H^+]^2([B] + [HL^-]_T - [HL^-]) - [H^+](K_w + K_1[CO_2(aq)] + 2K_a[HL^-]) - 2K_1K_2[CO_2(aq)] = 0 \quad (7)$$

where [B] is the concentration of base (NaOH) added, $[HL^-]_T$ is the total indicator concentration, $[CO_2(aq)]$ is the dissolved CO_2 concentration, K_1 and K_2 are the carbonic acid dissociation constants, and K_w and K_a are the water and indicator dissociation constants, respectively. The indicator pK_a was determined experimentally using low ionic strength buffers with quantified temperature dependence.[12] The equations for K_1, K_2, and K_w at zero salinity were taken from ref 13, and CO_2 solubility (K_H) reported in ref 14 was used to calculate $[CO_2(aq)]$ ($= K_H pCO_2$) for a given pCO_2 and temperature. A QuickBasic (Microsoft Corp., Redmond, WA) program was written to iteratively solve eq 7 for $[H^+]$ given the concentration of base added, total indicator concentration, and pCO_2.

METHODS

Spectrograph Design and Performance. As previously stated, one important goal of this research is to determine whether ROCS can be designed with an identical response for the same quantity of analyte. In absorbance-based ROCS, good absorbance accuracy, i.e., photometric accuracy, is fundamental to this goal. Knowing this, careful design and evaluation of the optical system is essential. The SAMI uses a miniature $f/2.5$ spectrograph with a 10 nm mm^{-1} reciprocal linear dispersion (model MS10, American Holographic, Littleton, MA) and three photodiode detectors (G1962 and S2386-5K, Hamamatsu Corp., Bridgewater, NJ). Detectors are positioned with the center wavelength at 434, 620, and 740 nm in the spectrograph focal plane. Detector photosensitive surface areas are 2.3, 2.4, and 2.4 mm^2 at 434, 620, and 740 nm, respectively, resulting in a resolution of ~23−24 nm. The detector size was selected to increase the S/N ratio without significantly compromising linearity due to inadequate resolution. The S/N ratio at 434, 620, and 740 is typically ~2500, 4500, and 4500, respectively.

Photometric accuracy in spectrophotometric measurements can be limited by stray light, and we initially underestimated the levels of stray light in our optical system. Tungsten light sources emit considerably more light in the near-infrared (NIR) than in the visible spectrum and measurements at short wavelengths, such as 434 nm, are especially susceptible to stray NIR light. Stray light levels, evaluated with a 600-nm long-pass filter, were found to be as high as 20% at 434 nm! A heat-absorbing filter (005GF13-25, Andover Corp., Salem, NH) placed at the spectrograph fiber optic input reduced stray light to 0.1%. Unfortunately the filter also significantly reduced the S/N at 740 nm. As an alternative to the heat-absorbing filter, a GaP photodiode (G1962, Hamamatsu) that is insensitive to NIR light was used in place of the broad-response Si photodiode at 434 nm. The GaP photodiode reduced stray light to less than 0.04% at 434 nm while maintaining a S/N of over 2500. As an additional check on absorbance accuracy, each spectrograph is routinely evaluated with neutral density filters. Absorbances typically agree with the filters to within ±0.003 au based on these evaluations, which is within the reproducibility of the neutral density filter measurements.

Spectrograph absorbance accuracy also depends on accurate wavelength calibrations. Each 620-nm detector output is optimized in the laboratory with a 620 ± 2 nm band-pass filter. The other detectors are positioned to correspond to 434 and 740 nm relative to the 620-nm detector, based on the grating dispersion. The broad absorbance bands (Figure 3) and detector band-pass relax the need for wavelength accuracy better than 2−3 nm.

Indicator Solution. A solution of 50.0 μM BTB with 42.0 μequiv L^{-1} NaOH was used for this study. The base is added to optimize the indicator pH response range.[5] The BTB and standardized NaOH were added to 1.00 kg of deionized, degassed H_2O, and the indicator solution was placed in polyethylene-coated aluminum bags (Pollution Measurement Corp., Oak Park, IL). The indicator solution composition was checked by equilibrating it with a known pCO_2 and measurement of R_{CO_2} on a UV/visible spectrophotometer.

Determination of the SAMI Experimental Response. The SAMI response (R_{CO_2}) is determined in a water-filled thermostated chamber. Variable gas concentrations are obtained by mixing a 1600 ppm CO_2 standard with CO_2-free air using two mass flow controllers.[5] The chamber headspace is continuously monitored by a nondispersive infrared CO_2 analyzer (NDIR) (model LI-6251, Li-COR, Inc., Lincoln, NE) calibrated with NIST traceable CO_2 gas standards (Air Liquide, Long Beach, CA). A circulating water pump mixes the equilibrator contents to ensure complete equilibration. Gas equilibration is slow due to the relatively large volume of water in the chamber (~2 L), with each CO_2 concentration requiring a minimum of 5 h to reach a stable headspace value. Equilibration temperature and barometric pressure are also monitored and used in the NDIR analyzer mole fraction (X_{CO_2}) calculation.[15] The NDIR pCO_2 is calculated using,

$$pCO_2 = X_{CO_2(wet)}P \quad (8)$$

where $X_{CO_2(wet)}$ is the CO_2 mole fraction in water-saturated air determined by the NDIR and P is the barometric pressure.

RESULTS

Sensor-to-Sensor Reproducibility. To test the predicted performance outlined above, three identically designed SAMIs

(12) Covington, A. K.; Whalley, P. D.; Davison, W. *Analyst* **1983**, *108*, 1528−1532.
(13) Millero, F. J. *Geochim. Cosmochim. Acta* **1979**, *43*, 1651−1661.
(14) Weiss, R. F. *Mar. Chem.* **1974**, *2*, 203-215.
(15) Wanninkhof, R.; Thoning, K. *Mar. Chem.* **1993**, *44*, 189−204.

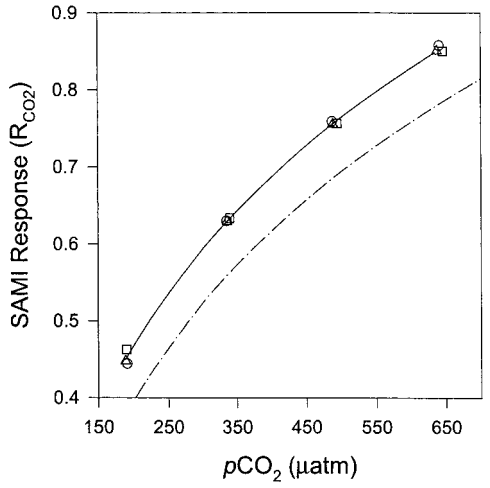

Figure 4. Response of three different SAMI-CO_2's obtained over ~1-week period in October 1997: ○, SAMI 5; □, SAMI 6; △, SAMI 7. The solid curve represents the best fit to the average of the three SAMI responses at each pCO_2 while the dashed−dotted curve represents the theoretical response calculated from eqs 5 and 7. Curves were fit to the equation $R_{CO2} = a(\log pCO_2)^2 + b(\log pCO_2) + c$. Coefficients from the individual curve fits are given in Table 1, and comparisons of pCO_2's calculated from the different SAMI curves are shown in Table 2.

were built in 1995 and each SAMI response was compared. These initial tests found that R_{CO_2} vs pCO_2 curves were not the same for each sensor. The instruments were constantly needed for field work, and they were not in the laboratory for sufficient time to rigorously examine and determine the source of the offsets. Over the following three years, whenever the SAMIs were in the laboratory steps were taken to reduce stray light, improve wavelength calibrations, prepare reproducible indicator solutions, and ensure complete CO_2 equilibration in the equilibration chamber, which were predicted to be the most likely sources of sensor-to-sensor response differences.

In 1997, three SAMIs were available for an extended period. Prior to determining the response curves, each SAMI was carefully tested for wavelength and photometric accuracy and the same indicator solution was loaded into the reagent bags for each instrument. The three SAMI responses were then sequentially determined. These results, presented in Figure 4, show a nearly identical response between the different instruments. The R_{CO_2} from the three SAMIs at 20.5 °C range from 0.45 to 0.85, or a pH change of ~0.40 (eq 5), from 200 to 650 μatm pCO_2. Coefficients from curve fitting are shown in Table 1, and the pCO_2s calculated for different R_{CO_2}'s using these equations are shown in Table 2. The estimated pCO_2s from the three response curves agree very well (1.8 μatm average standard deviation for the data in Table 2) in the range from 300 to 400 μatm, which is the most common range encountered in marine studies. Agreement at the curve extremes is not as good (6 μatm average SD) due to the sensitivity of the nonlinear curve fit with the limited number of standards (four). The SAMI 6 curve fit results are especially skewed at the low pCO_2 end due to a high data point. Incomplete equilibration between the water and headspace persists as a source of scatter in the response curves, and refinements in the equilibration procedure are needed to improve the reproducibility.

Table 1. Curve-Fitting Parameters for SAMI Response Data in Figures 4 and 9

coeff[a]	SAMI 5 10/29/97	SAMI 6 10/21/97	SAMI 7 10/23/97	theor curve	SAMI 5 01/11/98
a	0.1076	0.1913	0.1437	0.1369	0.1087
b	0.2391	−0.2444	0.0317	0.0655	0.2539
c	−0.6606	0.0264	−0.3682	−0.4798	−0.7015

[a] Coefficients from a curve fit of the form, $R_{CO_2} = a(\log pCO_2)^2 + b(\log pCO_2) + c$.

Table 2. Calculated pCO_2's (μatm) for Different R_{CO_2}'s Using the Equations in Table 1

R_{CO_2}	SAMI 5 10/29/97	SAMI 6 10/21/97	SAMI 7 10/23/97	SAMI 5 01/11/98	SD[a]
0.40	166	150	160	167	8.1
0.45	194	181	190	195	6.7
0.50	227	217	224	227	5.1
0.55	264	258	263	263	3.2
0.60	307	305	307	305	1.2
0.65	356	358	358	352	1.2
0.70	412	418	415	405	3.0
0.75	475	485	480	466	5.0
0.80	546	561	553	534	7.5
0.85	627	645	636	612	9.0

[a] This is the standard deviation of the calculated pCO_2 for SAMI 5, SAMI 6, and SAMI 7 in Figure 4.

The absorbance data used to generate Figure 4 illustrate the importance of using absorbance ratios (Figure 5). The absorbances differ between SAMIs by as much as 0.05 au. The consistently high and low absorbances between SAMIs suggest that the differences originate from optical path length differences, with SAMI 5 having the longest and SAMI 6 the shortest path length. The path length of the fiber optic cell (Figure 2) is 0.75 cm, but the path length can vary between SAMIs due to imprecise positioning of the fibers in the sealed fittings. Clearly, sensors that are based on absolute absorbances must have very carefully controlled path lengths to achieve reproducible sensor-to-sensor performance. As indicated by the convergence of the response curves in Figures 4 and 5, the SAMI response (R_{CO_2}) is insensitive to path length variability.

Comparison with the Theoretical Response. The sensor theoretical response calculated from eqs 5 and 7 is plotted with the experimental response in Figure 4. Table 1 includes the coefficients of the theoretical equation. The predicted and actual curves are very similar in shape but do not quantitatively match. The similarity in curve shapes provides evidence that there are no instrument-related deviations in the SAMI response over the measured pCO_2 range. The observed offset could originate from inaccuracy in the thermodynamic constants for BTB and CO_2. Debye−Hückel approximations of the BTB activity coefficients provide evidence that the difference between the ionic strength (μ) of the buffers ($\mu = 0.023$ M) used to determine the BTB pK_a and the indicator solution ($\mu < 1 \times 10^{-4}$ M) could cause an error greater than 0.1 in the pK_a. The pK_a was not corrected to the indicator solution ionic strength because of the inaccuracy of the calculated activity coefficients. The correction would, however, increase the predicted R_{CO_2}, supporting that the ionic strength difference is the source of the offset. Further work to

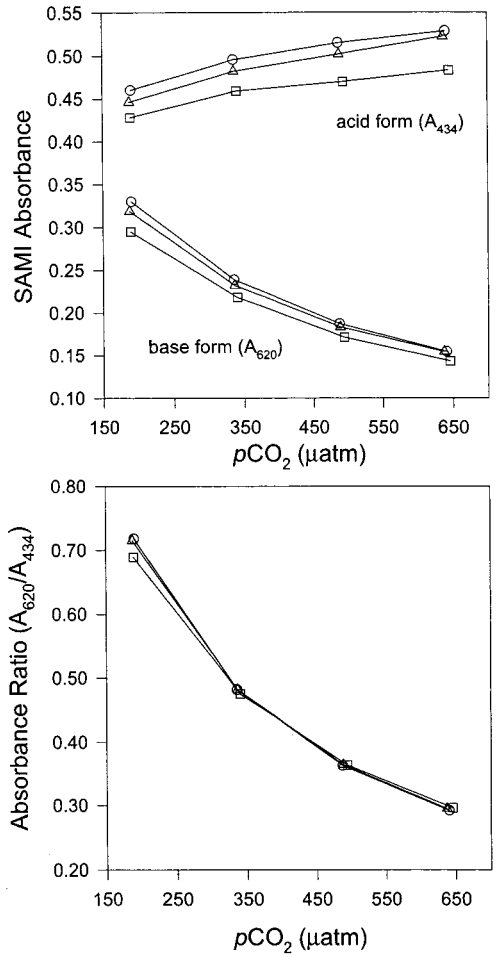

Figure 5. SAMI absorbances (top) and absorbance ratio A_R (bottom) used to calculate R_{CO_2} in Figure 4: ○, SAMI 5; □, SAMI 6; △, SAMI 7.

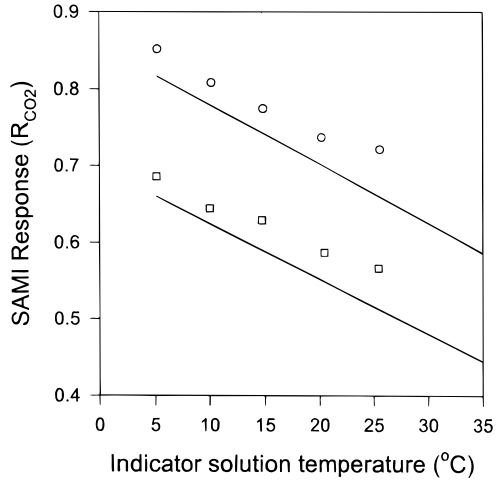

Figure 6. Experimental and theoretical temperature response at 325 (□) and 506 μatm (○). The theoretical curves (solid lines) at 325 and 506 μatm have slopes of 0.0071 and 0.0076 R_{CO_2} unit °C^{-1}, respectively. The experimental data curves (not shown) at 325 and 506 μatm have slopes of 0.0058 and 0.0065 R_{CO_2} unit °C^{-1}, respectively.

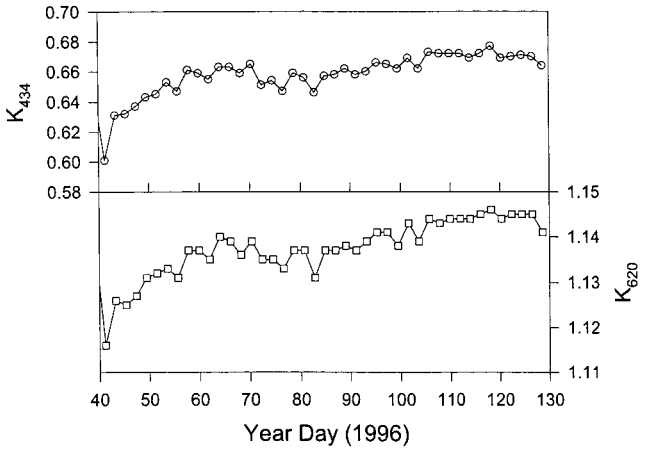

Figure 7. Blank constant (K_λ) from SAMI 6 at 434 (top) and 620 nm (bottom) during a long-term mooring deployment off Cape Hatteras, NC, in 1996.

obtain a more accurate estimate of the pK_a at low ionic strength is underway.

Most chemical sensors have a temperature-dependent response and it is important to accurately quantify this dependence and correct for it in the recorded signal. The SAMI temperature response was evaluated by determining both the experimental and theoretical R_{CO_2} at different temperatures and pCO_2's (Figure 6). The sensor temperature dependence originates primarily from the temperature-dependent CO_2 solubility (a solution equilibrated with the same pCO_2 will have a different pH at different temperatures). R_{CO_2} decreases as temperature increases as a result of this effect. The experimental temperature response follows the expected trend (Figure 6) although the offset is present between the experimental and theoretical R_{CO_2}'s as discussed above. The implications of Figure 6 are that the temperature coefficient is significant and that the magnitude depends on the pCO_2. During previous field deployments, the SAMIs have been calibrated as closely as possible to the expected seawater temperature to minimize the temperature correction.

Evaluation of Long-Term Stability. A reproducible sensor-to-sensor response as shown in Figure 4 is one performance characteristic necessary for calibration-free operation. A second equally important quality is that the response must not change, or drift, over time. Drift is minimized in the SAMIs using three techniques: renewing the indicator reagent, periodic measurement of solution blanks, and use of absorbance ratios. Blanks are necessary not only to calculate absorbances but also to correct for wavelength-dependent intensity changes that cause the relationship between I_0 and I_{ref} to change over time (eq 6). A record of the K_λ's from a mooring deployment off Cape Hatteras, NC, illustrates the significance of this problem (Figure 7). Over the 90-day record, the K_{434} and K_{620} change by 11 and 2.5%, respectively. If K_λ was only obtained at the beginning of the study and was assumed to remain constant, an error of as much as 0.060 R_{CO_2} unit, or ~50 μatm pCO_2, would result by the end of the time period.

Drift improvements by renewing the reagent, measuring blanks, and using absorbance ratios have not been systematically compared to the performance of ROCS that do not employ these techniques. However, an indirect comparison is provided from the literature where sparse long-term stability data have been reported for nonrenewable intensity-based ROCS (see for example the recent SPIE volume *Chemical, Biochemical and Environmental*

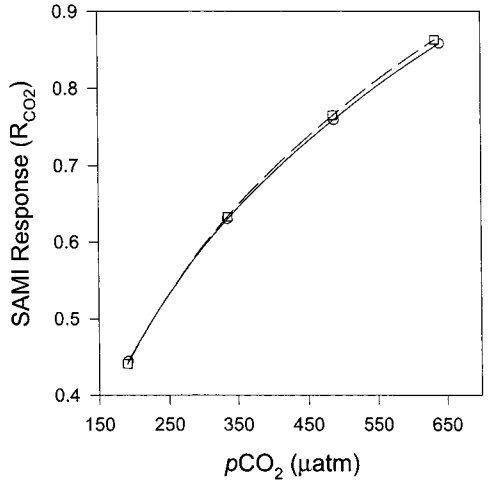

Figure 8. SAMI 5 response curves for data from 10/29/97 (Figure 4) (○) and 74 days later on 1/11/98 (□). The 10/29/97 and 1/11/98 regression curves are shown as solid and dashed lines, respectively. Coefficients from the curve fits are given in Table 1.

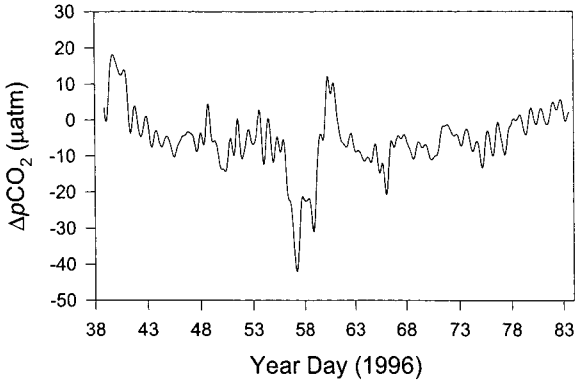

Figure 9. Difference in pCO_2 determined at a single location but at two different depths on an ocean mooring off Cape Hatteras, NC. The data were first low-pass filtered to improve the figure clarity (reduce short-term variability). The ΔpCO_2 is equal to SAMI 5 (10 m) − SAMI 6 (22 m). The difference is calculated over the period when both instruments were operational (SAMI 5 stopped functioning near year day 83 due to an electronic problem).

Fiber Sensors IX, June 1997). This summary is based on the criterion that a rigorous evaluation of long-term stability consists of regular accuracy checks without recalibration for a period greater than 1 week. A more specific example is given by examination of ROCS CO_2 sensors developed for oceanographic applications.[16−18] Almost no long-term data have been presented for these sensors, which are all based on fixed reagents. In contrast, the SAMIs have demonstrated excellent stability from the very early stages of development.[4,5] A month-long in situ seawater test found no detectable drift in the response,[5] and recent laboratory studies have shown no significant change in the response with time (Figure 8). Although the two curves in Figure 8 are not identical, the difference in pCO_2 determined from the curve fit equations is very small over the typical oceanographic range (Table 2). Verification of accuracy during ocean mooring deployments has been more difficult due to infrequent visits by supporting research vessels and spatial variability between the ship and mooring. However, two SAMIs that were deployed on an ocean mooring off Cape Hatteras during 1996 give an indication of the long-term stability in the field (Figure 9). The two pCO_2 signals, which were calculated from the same $R_{CO_2}-pCO_2$ response curves, show no systematic deviation with time over the ∼50 days when the two instruments were operational. The large periodic differences between the two instruments correspond to temperature differences between the instrument depths indicating the presence of density stratification and associated concentration gradients with depth (DeGrandpre, M. D., unpublished, 1998). The combined data sets in this case provide an evaluation of the long-term stability in the field.

It should be noted however that the SAMIs are not completely immune to drift. Biofouling can create anomolous results during prolonged deployments in shallow, productive coastal waters (DeGrandpre, M. D., unpublished results, 1998). In most SAMI-CO_2 studies, membrane biofouling has been minimal. Preventative measures such as the use of biocide-impregnated polymers can help reduce systematic errors due to biofouling in productive waters.

DISCUSSION AND CONCLUSIONS

The results from this study demonstrate the potential for calibration-free ROCS. The SAMI-CO_2 response is both reproducible between instruments and very stable, two essential criteria for calibration-free operation. Although the SAMI departs from the conventional single-ended optrode design, similar performance could be expected for optrodes *if* the optrode is configured as in conventional colorimetric measurements, i.e., where the reagent is renewed and true solution absorbances are determined. Nonrenewable ROCS have no means for determining I_0 and can therefore not take advantage of the improved performance offered by this approach. However, most fixed reagent sensor designs can be readily modified to accommodate the pump, valve, and additional tubing. A wide variety of pumping mechanisms and valves are now available,[19,20] and they have proven to be very reliable for long-term measurements in harsh environments.

To eliminate dependence on the system operational parameters such as path length, light intensity, and the detector response function, ratio techniques need to be employed. Multiwavelength detection and use of absorbance ratios is a very powerful approach that takes advantage of the two forms of a colorimetric reagent. Many colorimetric ROCS sensors utilize reagents of this type including those for pH,[21] gases,[22] and metal ions[23,24] to name a few.

Calibration-free operation is also facilitated if the sensor response is based on an equilibrium between the reagent solution and external sample. The sensor response becomes diffusion-

(16) Goyet, C.; Walt, D. R.; Brewer, P. G. *Deep-Sea Res.* **1992**, *39*, 1015−1026.
(17) Goswami, K.; Kennedy, J. A.; Dandge, D. K.; Klainer, S. M.; Tokar, J. M. *Proc. SPIE-Int. Soc. Opt. Eng.* **1990**, *1172*, 225−232.
(18) Lefevre, N.; Ciabrini, J. P.; Michard, G.; Brient, B.; DuChaffaut, M.; Merlivat, L. *Mar. Chem.* **1993**, *42*, 189−198.
(19) Jannasch, H.; Johnson, K. S.; Sakamoto, C. M. *Anal. Chem.* **1994**, *66*, 3352−3361.
(20) Weeks, D. A.; Johnson, K. S. *Anal. Chem.* **1996**, *68*, 2717−2719.
(21) Peterson, J. I.; Goldstein, S. R.; Fitzgerald, R. V.; Buckhold, D. K. *Anal. Chem.* **1980**, *52*, 864−869.
(22) Zhou, Q.; Kritz, D.; Bonnell, L.; Sigel, G. *Appl. Opt.* **1989**, *28*, 2022−2025.
(23) Chau, L.-K.; Porter, M. D. *Anal. Chem.* **1990**, *62*, 1964−1971.
(24) Radloff, D.; Matern, C.; Plaschke, M.; Simon, D.; Reichert, J.; Ache, H. J. *Sens. Actuators B* **1996**, *35−36*, 207−211.

independent in this case and is insensitive to changes in the diffusional boundary layer around the sensor membrane. This simplification also makes it possible to model the response solely on the basis of thermodynamic considerations. If the thermodynamic constants are available, such models are useful for evaluating the sensor response and detecting systematic measurement errors.

Many ROCS are based on fluorescent reagents.[2] These sensors appear to present a greater challenge for calibration-free operation because there is no readily accessible equivalent to absorbance. The fundamental response depends on the fluorophore quantum efficiency and concentration. But, as in any intensity-based measurement, the signal output also reflects the detector response, light source output, and additional instrumental parameters.[25] A fluorescence ratio of two forms of the fluorophore can be used,[26] but since the two forms are detected at different wavelengths, the ratio would not correct for wavelength-dependent throughput and detector response, an obstacle to designing sensors with an identical response. If the fluorophore does not exist in two forms, as found in quenching-based O_2 sensors[27−29] the ratio approach could only be used if an additional O_2-insensitive fluorophore was included in the sensing solution. With all of these considerations, it is evident that development of identical fluorescence-based ROCS may be quite challenging. However, good long-term stability may still be achievable by using the ratiometric approach.

All calibration-free sensors would still require initial characterization of the response. After the response is thoroughly evaluated and well-established, a single set of regression coefficients could be used to calculate analyte concentration from any one of the identically designed sensors. Calibration-free sensors would also undoubtedly require occasional checks on the instrument response. A single calibration standard could be used to determine whether the instrument response matches the expected response, and if they do not agree, further evaluation of the instrument optical system or indicator chemistry would be necessary.

Calibration-free ROCS may also be developed based on other approaches. Fluorescence lifetime-based ROCS are one example of a promising alternative.[30] Furthermore, the performance of nonrenewable ROCS continues to be improved through innovative fabrication techniques.[27,29] Although ROCS have not provided the easy solution to chemical sensor problems that researchers had hoped, development efforts that deal realistically with ROCS limitations, combined with a lot of determination, can result in sensors suitable for real-world applications.

(25) Ingle, J. D.; Crouch, S. R. *Spectrochemical Analysis*; Prentice Hall: Englewood Cliffs, NJ, 1988.
(26) Thompson, R. B.; Jones, E. R. *Anal. Chem*. **1993**, *65*, 730−734.
(27) McDonagh, C.; MacCraith, B. D.; McEvoy, A. K. *Anal. Chem*. **1998**, *70*, 45−50.
(28) Wolfbeis, O. S.; Posch, H. E.; Kroneis, H. W. *Anal. Chem*. **1985**, *57*, 2556−2561.
(29) Klimant, I.; Meyer, V.; Kühl, M. *Limnol. Oceanogr*. **1995**, *40*, 1159−1165.
(30) Draxler, S.; Lippitsch, M. E. *Proc. SPIE-Int. Soc. Opt. Eng.* **1993**, *2085*, 61−67.

ACKNOWLEDGMENT

This research has been funded by the Department of Energy Ocean Margins Program and NSF-Ocean Sciences. We would especially like to thank Dr. Curtis Olsen (formerly of the DOE) for supporting funding of this work in its early stages.

Received for review May 29, 1998. Accepted December 18, 1998.

AC9805955